ACS OMEGA

http://pubs.acs.org/journal/acsodf

Article

# Theoretical Study on a Supramolecular Dimeric Structure Constructed by Metallofullerene $Y_3N@C_{80}$ and Figure-of-Eight Nanoring

Linshan Liu,[‖] Yang Liu,[‖] Zhuxia Zhang,* and Taishan Wang*

Cite This: *ACS Omega* 2023, 8, 23754−23762

Read Online

ACCESS | Metrics & More | Article Recommendations | Supporting Information

**ABSTRACT:** A new supramolecular complex with a dimeric structure ($2Y_3N@C_{80}$⊂OPP) constructed by metallofullerene $Y_3N@I_h$-$C_{80}$ and figure-of-eight molecular nanoring of oligoparaphenylene (OPP) was investigated using dispersion-corrected density functional theory (DFT-D3). The interactions between the $Y_3N@I_h$-$C_{80}$ guest and the OPP host were studied theoretically at the B3LYP-D3/6-31G(d)∼SDD level. By analyzing geometric characteristics and host−guest binding energies, it is revealed that the OPP is an ideal host molecule for the $Y_3N@I_h$-$C_{80}$ guest. Typically, the OPP can well induce the orientation of the endohedral $Y_3N$ cluster on the plane of nanoring. Meanwhile, the configuration of the dimeric structure demonstrates that OPP presents excellent elastic adaptability and shape flexibility during the encapsulation of $Y_3N@I_h$-$C_{80}$. Highly accurate binding energy suggests that $2Y_3N@C_{80}$⊂OPP (∼−443.82 kJ $mol^{-1}$ at the ωB97M-V/def2-QZVPP level of theory) is an extremely stable host−guest complex. Thermodynamic information indicates that the formation of the $2Y_3N@C_{80}$⊂OPP dimer is thermodynamically spontaneous. Furthermore, electronic property analysis reveals that this dimeric structure has a strong electron-attracting ability. Energy decomposition and real-space function analyses of host−guest interactions reveal the characteristics and nature of the noncovalent interactions in the supramolecules. These results provide theoretical support for the design of new host−guest systems based on metallofullerene and nanoring.

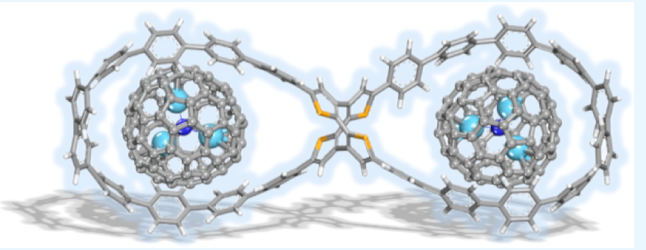

## 1. INTRODUCTION

Endohedral metallofullerenes are metal−carbon hybrid molecules with interesting core−shell structures, with metallic species (atoms or clusters) imprisoned in carbon cages.[1] Since their discovery, metallofullerenes have been found to have a wide variety of applications in different fields, such as biomedical imaging, solar energy conversion, and electronic devices.[2−4] In addition, metallofullerenes have significant applications in chemistry and materials. Among them, the construction of supramolecular complexes based on metallofullerenes is one of the most active fields.[5]

Carbon nanorings are a kind of representative host to accommodate metallofullerene and modulate the physical and chemical properties.[6] As a type of concave receptor, carbon nanorings can encapsulate the convex surface of metallofullerenes and maximize stabilization through so-called concave−convex π−π interactions. The most representative examples of carbon nanorings are cyclophenylpropylenes (CPPs), which consist of phenylene units that are para-linked in a cyclic manner and represent the shortest fragment of an [*n*, *n*]armchair carbon nanotube. After the discovery of $C_{60}$ being trapped in [10]CPP by Yamago et al.,[7] the following class of host−guest supramolecular systems has received great attention: $C_{59}N$⊂[10]CPP,[8] $C_{70}$⊂[10−11]CPP,[9] La@$C_{82}$⊂[11]CPP,[10] Gd@$C_{82}$⊂[11]CPP,[11] etc.

Since the landmark synthesis of [9]-, [12]-, and [18]CPP in 2008,[12] a diversity of [*n*]CPPs and more CPP derivatives have been developed, including lemniscates,[13] cylinders,[14] propellers,[15] and catenanes.[16] Derivatives of CPPs have facilitated the discovery of macrocyclic conjugated structures, which often have unique nanoscale cavities that can be used for supramolecular assembly. From the perspective of molecular design, two CPPs can be fused with different linkers to assemble a fully conjugated figure-of-eight nanoring. Recently, a novel figure-of-eight nanoring of oligoparaphenylene (OPP) has been reported. The molecular skeleton consists of two [10]paraphenylene loops and a cyclooctatetrathiophene.[17] The remarkable thing about this macrocycle is that its two cavities can each house a molecule, such as fullerenes $C_{60}$ and $C_{70}$, through noncovalent interactions to form peanut-like 1:2

Received: March 27, 2023
Accepted: May 19, 2023
Published: June 16, 2023





https://doi.org/10.1021/acsomega.3c02049
*ACS Omega* 2023, 8, 23754−23762

host−guest complexes, which have been demonstrated and characterized by X-ray crystallography.[17] Therefore, it is interesting to explore more supramolecular complexes based on this figure-of-eight nanoring of OPP.

It has been recently shown that [12]CPP is suitable for encapsulating $C_{80}$-based metallofullerenes and forming stable host−guest complexes.[18−25] Notably, the cavity sizes of OPP and [12]CPP are relatively close, so it is possible to hoop $C_{80}$-based metallofullerenes with OPP. As mentioned above, metallofullerenes have richer physical and chemical properties than hollow fullerenes. Notably, compared to hollow fullerene $C_{70}$, which also has thermally activated delayed fluorescence (TADF) properties, $Y_3N@C_{80}$ holds a smaller $S_1-T_1$ energy gap ($\Delta E_{ST}$), which allows $T_1$ excitons to be transferred back to $S_1$ excitons by reverse intersystem crossing,[26] resulting in stronger fluorescence emission. Therefore, $Y_3N@C_{80}$ offers the possibility of using itself as a TADF material for applications such as OLEDs.[27] It is meaningful to construct a peanut-like 1:2 host−guest complex based on metallofullerenes and this figure-of-eight nanoring to study the changed properties in this dimeric structure.

In this study, we explored a new supramolecular complex with a dimeric structure constructed by metallofullerene $Y_3N@I_h$-$C_{80}$ and a figure-of-eight molecule of OPP by means of density functional theory (DFT) calculations. Two supramolecular systems of $Y_3N@C_{80}$⊂OPP and $2Y_3N@C_{80}$⊂OPP were theoretically assessed (hereafter the $I_h$-prefix is omitted for simplification). The results of this study can provide important information for understanding the structure and properties of this kind of supramolecular complex.

## 2. COMPUTATIONAL METHODS

All of the geometric optimizations were carried out by the B3LYP-D3 method within the 6-31G(d)∼SDD level [the 6-31G(d) basis set for C, H, and S atoms; the MWB28 basis set for Y atoms].[28−30] Here, Grimme's DFT-D3 method,[31] which provides an empirical dispersion correction for DFT, was employed for the present study. Then, harmonic frequency analyses were performed at the same level to confirm whether those structures were local minima or transition states on the potential energy surface. Geometry optimizations and frequency analyses were implemented by the Gaussian 09 program.[32]

To obtain accurate binding energy for supramolecular complexes, the ωB97M-V functional in combination with a very large def2-QZVPP basis set was employed in single-point calculations.[33,34] The ωB97M-V is fairly accurate for evaluating intermolecular interactions,[35] and single-point calculations were conducted using the ORCA 5.0.3 program[36] via the RIJCOSX technique[37] to accelerate the calculations.

The electrostatic potential (ESP), energy decomposition analysis based on forcefield (EDA-FF), and independent gradient model based on Hirshfeld partition (IGMH) analyses were all finished by Multiwfn 3.8 (dev) code.[38−41] Thermochemical properties were calculated by the Shermo package.[42]

## 3. RESULTS AND DISCUSSION

**3.1. ESP Analysis and Geometric Configurations ($Y_3N@C_{80}$⊂OPP and $2Y_3N@C_{80}$⊂OPP).** The ESP of a molecule represents the interaction energy per unit charge at a given position between the molecule and an external environment, without considering the effects of charge transfer and polarization. The red (blue) area represents the surface local maxima (minima) of the ESP (as shown in Figure 1).

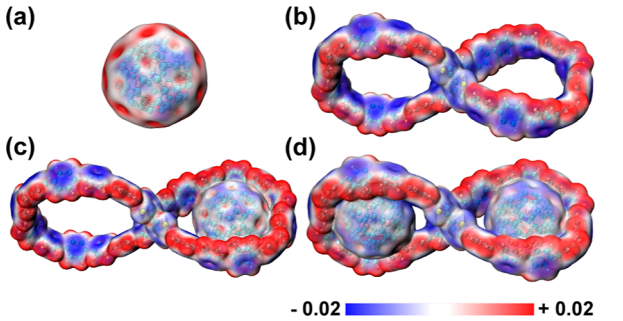


**Figure 1.** ESP diagram of the van der Waals surface: (a) $Y_3N@C_{80}$, (b) OPP, (c) $Y_3N@C_{80}$⊂OPP, and (d) $2Y_3N@C_{80}$⊂OPP. The color scale is given in a.u.

To elucidate the interactions between the two systems, the ESP of the system was analyzed (Figure 1a−d). The OPP displayed negative regions associated with phenyl rings, while the edges of the ring showed positive regions due to the presence of hydrogen atoms (Figure 1b). Therefore, the cavity was mostly negative, which would be favorable for accommodating electron-deficient species. According to previous studies, $C_{60}$ and $C_{70}$ exhibited nearly zero ESP, with only very slight positive regions observed in $C_{76}$ and $C_{78}$. Nevertheless, the presence of metal clusters in the endofullerenes introduced a greater degree of asymmetry in charge distribution, resulting in fairly pronounced positive and negative regions in the ESP.[43] $Y_3N@C_{80}$ (Figure 1a) appeared to have a markedly positive region where the Y atom is in contact with the carbon cage, while the carbon cages near the N atom of the $Y_3N$ cluster showed a negative region. This was similar to the ESP behavior of $Sc_2C_2@C_{2n}$ ($n$ = 40, 41, and 42).[19]

In addition, the size effect is a crucial factor influencing the self-assembly of host−guest molecules. The $Y_3N$ metal cluster is encapsulated by the $C_{80}$ cage to form a stable $C_{80}$-based metallofullerene, $Y_3N@C_{80}$. The diameter of $Y_3N@C_{80}$ is approximately 8 Å, and OPP has two nanoscale cavities, which are ellipsoidal in shape with a long axis length of approximately 19.43−19.50 Å and a short axis length of approximately 14.33−14.40 Å. This provides the possibility for both to form host−guest supramolecular complexes (1:1 and 1:2). Figure 2 shows the most stable structures found for the complexes of OPP with the $Y_3N@C_{80}$ ($Y_3N@C_{80}$⊂OPP and $2Y_3N@C_{80}$⊂OPP) considered in this work. For the $Y_3N@C_{80}$⊂OPP complex, $Y_3N@C_{80}$ fits nicely within the cavity of OPP and establishes excellent interactions with all phenyl units. The orientation of the endofullerene in the cavity places the endohedral Y atom on the plane of the nanoring, which means that the carbon atoms always face the phenylacetylene ring when interacting with the endohedral unit. The $2Y_3N@C_{80}$⊂OPP complex displayed similar features, and the $Y_3N$ cluster encapsulated in the $C_{80}$ cage was relatively fixed in position in the complex and almost coincided with the plane of the ring. However, the structure is less stable relative to the other directions of the host, which is possibly due to the asymmetry of the electron charge, as shown in Figure 1a−d. The ESP of the endofullerene is more pronounced in the region where the endohedral unit contacts the carbon cage.


https://doi.org/10.1021/acsomega.3c02049
ACS Omega 2023, 8, 23754−23762

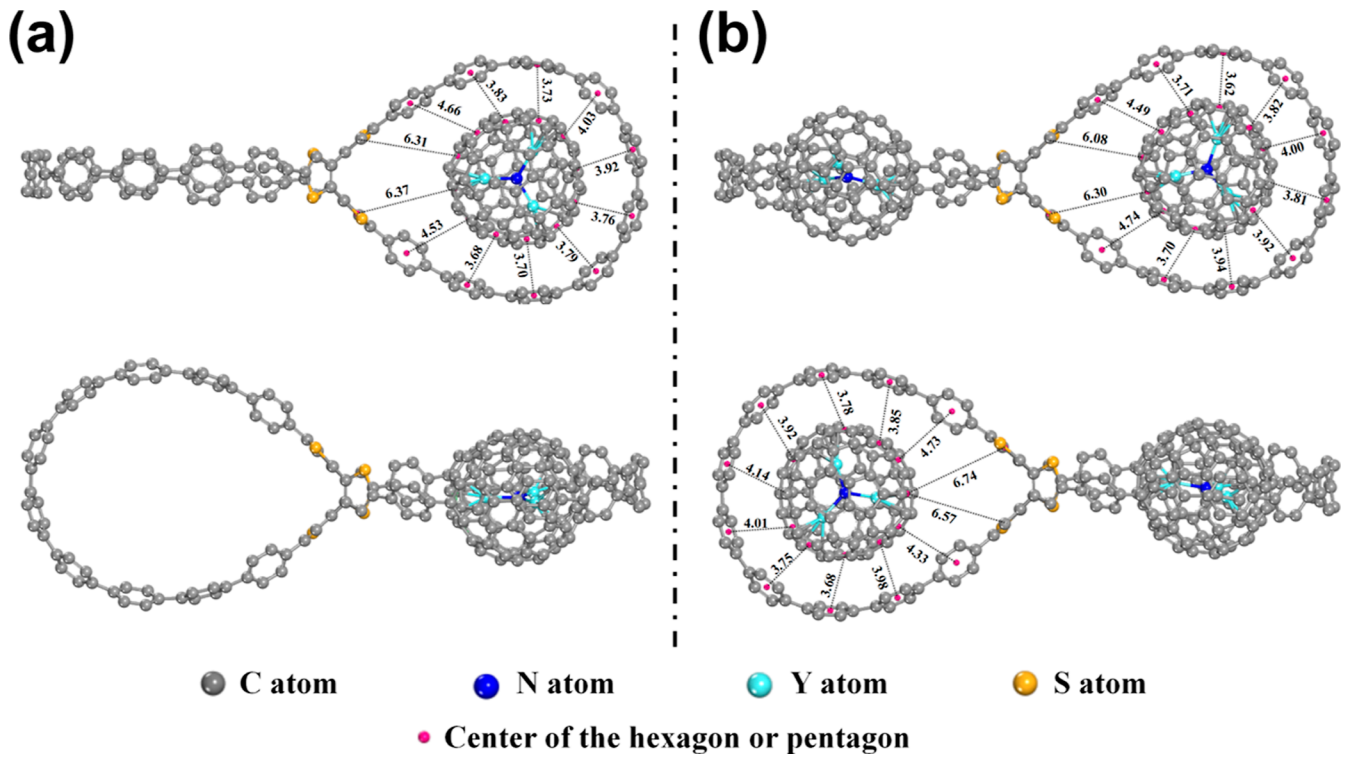


**Figure 2.** Interfacial distances ($d_i$) between host and guest of (a) $Y_3N@C_{80}$⊂OPP and (b) $2Y_3N@C_{80}$⊂OPP.

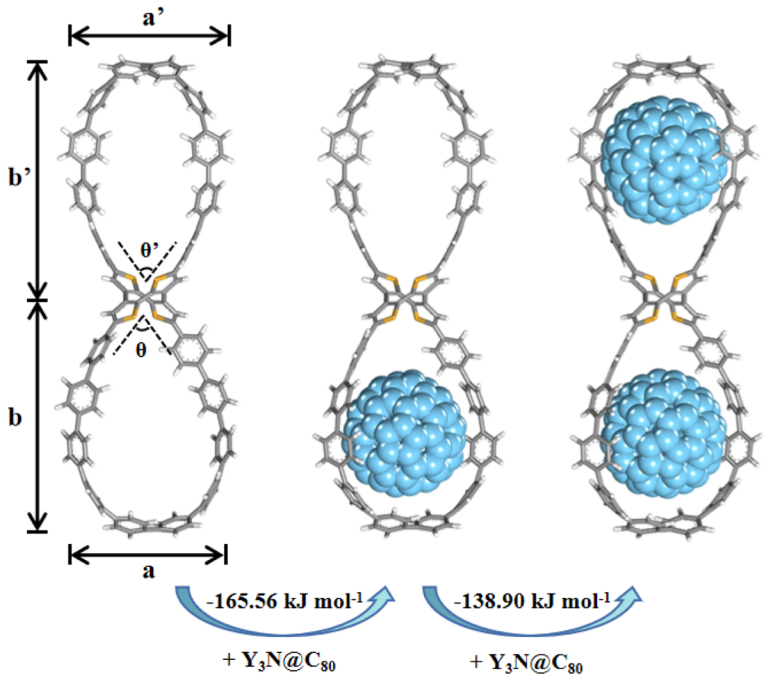


| | a (Å) | b (Å) | θ (°) | a' (Å) | b' (Å) | θ' (°) | Dipole (Debye) |
|---|---|---|---|---|---|---|---|
| $Y_3N@C_{80}$⊂OPP | ⇧14.94 | ⇩19.00 | ⇧88.77 | 14.38 | 19.44 | 89.44 | 0.72 |
| OPP | 14.33 | 19.50 | 84.22 | 14.40 | 19.43 | 90.74 | 0.13 |
| $2Y_3N@C_{80}$⊂OPP | 15.01 | 18.98 | 83.30 | ⇧14.94 | ⇩19.06 | ⇧96.02 | 0.59 |

**Figure 3.** Configurations, geometric parameters, and dipole moment information of metallofullerene complexes optimized by DFT.



https://doi.org/10.1021/acsomega.3c02049
*ACS Omega* 2023, 8, 23754−23762

Considering that the ESP of the edge of the OPP cavity has a noticeable negative charge, the metallofullerene is oriented such that its positive charge region faces the negative charge region of the host. The configuration of this complex is consistent with previous studies of supramolecular systems of three metal nitride fullerenes ($DyY_2N@C_{80}$⊂[12]CPP, $Y_3N@C_{80}$⊂[12]CPP, and $Sc_3N@C_{80}$⊂[11]CPP).[22,25,43] Hence, from an electrostatic point of view, the $C_{80}$-based fullerenes would be oriented with the endohedral atoms on the plane of OPP, thus allowing complementary ESP regions to be in close contact (Figure 1c,d).[43]

Figure 2 also shows the interface distance ($d_i$) between the host and guest. Here, $d_i$ means the interfacial distance between the centroid of a ring unit of the host and the nearest centroid of a hexagon or pentagon of an endofullerene. The $d_i$ values for $Y_3N@C_{80}$⊂OPP and $2Y_3N@C_{80}$⊂OPP were 3.68−6.37 Å (Figure 2a) and 3.62−6.74 Å (Figure 2b), respectively, with a wide distribution. This indicates that the attraction between the endofullerene and OPP is not uniform. The narrower the interface is, the stronger the interaction between $Y_3N@C_{80}$ and OPP, as the interface distance is not significantly larger than the vdW distance between graphene sheets (3.4 Å).

To further evaluate the noncovalent interactions and shape flexibility of OPP, the geometrical parameters and dipole moments of the OPP host and its main guest complexes are detailed in Figure 3. Calculated Gibbs free energies indicate that the formation of the host−guest complexes is thermodynamically favorable, with 165.56−138.90 kJ mol$^{-1}$ downhill for each additional $Y_3N@C_{80}$ hosted by OPP (detailed parameters listed in Table 1). When the host−guest forms a 1:1 fullerene complex, the cavities of the OPP become shorter by approximately 0.50 Å and narrower by approximately 0.61 Å, with these slight shape changes occurring simultaneously with an increase of approximately 5° in the thiophene dihedral angle. The resulting deformation energy of the ring compensates for the noncovalent host−guest interactions, allowing the host OPP to adopt a more compressed and curved shape to better accommodate the convex guest molecule. Meanwhile, the geometry of the other cavity of the OPP remains nearly unchanged. When the second $Y_3N@C_{80}$ is complexed, similar geometric changes occur in the latter cavity, becoming shorter and wider as the thiophene dihedral angle increases. Notably, this is in contrast to the changes in the optimized $2C_{60}$@OPP and $2C_{70}$@OPP complexes[17] (the host OPP cavity becomes longer and narrower as the thiophene dihedral angle decreases), indicating that the figure-of-eight nanoring OPP can cleverly arrange slightly different shapes for larger-volume $C_{80}$-based metallofullerenes, demonstrating the adaptability and shape flexibility of OPP. Furthermore, the effect of the host molecule on the endohedral unit is also of concern. As previously mentioned, $Y_3N$ is planar in both the metallofullerene and the complexes, and the Y−N distances and the Y−N−Y angles are not significantly different (as shown in Table S1), indicating that the weak interaction between the host and the guest did not significantly affect the endohedral cluster.

**Table 1. Binding Energies ($\Delta E$, kJ mol$^{-1}$) between $Y_3N@C_{80}$ and OPP, the Changes of Gibbs Free Energy ($\Delta G$, kJ mol$^{-1}$), Enthalpy ($\Delta H$, kJ mol$^{-1}$), and Entropy ($\Delta S$, J mol$^{-1}$ K$^{-1}$) of the Formations of the 1:1 and 1:2 Complexes**

| complexes | $\Delta E^a$ | $\Delta G$ | $\Delta H$ | $\Delta S$ |
|---|---|---|---|---|
| $Y_3N@C_{80}$⊂OPP | −233.99 | −165.56 | −226.63 | −204.83 |
| $2Y_3N@C_{80}$⊂OPP | −443.82 | −304.46 | −429.99 | −421.05 |

[a]Obtained at the ωB97M-V/def2-QZVPP level//B3LYP-D3/6-31G(d)∼SDD level.

Furthermore, due to the quasi-symmetry of OPP, free OPP has a small dipole moment of almost zero (0.13). However, all the host−guest complexes are polar supramolecules with certain dipole moments as a result of the electron-rich nature of the main guest and the electron-deficient nature of the guest metallofullerene.

**3.2. Binding Energies and Thermodynamic Properties.** Binding energy is very valuable and decisive for measuring the stability and strength of intermolecular noncovalent interactions of supramolecular systems. Table 1 lists the binding energies ($\Delta E$) calculated at the ωB97M-V/def2-QZVPP level. For the $Y_3N@C_{80}$⊂OPP complex, $\Delta E$ is approximately −233.99 kJ mol$^{-1}$. In addition, it is noted that $\Delta E$ in $2Y_3N@C_{80}$⊂OPP is close to twice that of the $Y_3N@C_{80}$⊂OPP complex, which is due to the larger π−π contact regions of the host−guest molecule. Furthermore, it is important to note that the binding energy of $2Y_3N@C_{80}$⊂OPP is significantly larger than that of the $2C_{60}$@OPP and $2C_{70}$@OPP systems,[17] indicating that OPP exhibits higher stability in encapsulating $C_{80}$-based metallofullerenes. Apparently, the design of efficient fullerene receptors mainly relies on favorable dispersion interactions in an attempt to maximize the contact surface between the fullerene and the host molecule.[43−46] The incorporation of $Y_3N@C_{80}$ into the complex system increases the π−π contact area, thereby enhancing the host−guest interactions. In order to provide more information about the suitability of the OPP cavity, the binding of $Y_3N@C_{80}$ and [11]CPP was calculated and the relative stability of the complexes studied in this work was compared. The binding energy of $Y_3N@C_{80}$⊂[11]CPP was estimated at the very accurate ωB97M-V/def2-QZVPP level and is −238.90 kJ mol$^{-1}$, which is between $Y_3N@C_{80}$⊂OPP (−233.99 kJ mol$^{-1}$) and $2Y_3N@C_{80}$⊂OPP (−443.82 kJ mol$^{-1}$).

The thermodynamic information of the encapsulations of $Y_3N@C_{80}$ by the OPP at 298.15 K and 1 atm obtained by using DFT calculations at the B3LYP-D3/6-31G(D)∼SDD level of theory is also given in Table 1. The relative order of $\Delta G$ and $\Delta H$ for the 1:1 and 1:2 complexes is consistent with the relative order of $\Delta E$. The binding of $Y_3N@C_{80}$ and OPP is spontaneous, with $\Delta G$ values of −165.56 and −304.46 kJ mol$^{-1}$ for $Y_3N@C_{80}$⊂OPP and $2Y_3N@C_{80}$⊂OPP, respectively. For the 1:2 complex, the $\Delta G$ of $2Y_3N@C_{80}$⊂OPP is larger than that of $Y_3N@C_{80}$⊂OPP, indicating that the OPP molecule is more likely to bind two $Y_3N@C_{80}$ to form 1:2 complexes. Based on the $\Delta H$ value, both complex formation reactions are exothermic, with the enthalpy contribution arising from the reduction of intermolecular interaction forces and the resulting decrease in the internal energy of the system. The free molecules decreased after the formation of the host−guest complexes, and correspondingly, the entropies of the two complexes decreased by −204.83 to −421.05 J mol$^{-1}$ K$^{-1}$. All of this thermodynamic information indicates that the binding of $Y_3N@C_{80}$ to OPP in the vacuum was enthalpy-driven and entropy-opposed.

**3.3. Frontier Orbital Features and Electronic Properties.** It is well known that the frontier molecular orbitals include the highest occupied molecular orbital (HOMO) and


https://doi.org/10.1021/acsomega.3c02049
ACS Omega 2023, 8, 23754−23762

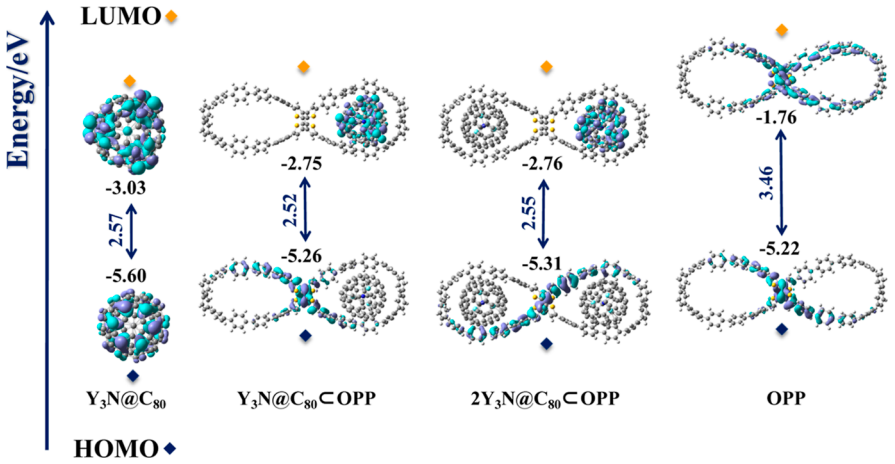


**Figure 4.** Frontier molecular orbital and the corresponding energy level diagram of $Y_3N@C_{80}$, $Y_3N@C_{80}$⊂OPP, $2Y_3N@C_{80}$⊂OPP, and OPP.

the lowest unoccupied molecular orbital (LUMO), and the electrons in the frontier orbitals, such as the valence electrons in atoms, are the core of molecular reactions. Figure 4 shows the composition and energy levels of the frontier orbitals of $Y_3N@C_{80}$ and OPP in the 1:1 and 1:2 complexes. The frontier orbital gap of OPP was much larger than that of $Y_3N@C_{80}$ and their complexes. The HOMOs of the complexes are completely derived from the HOMO of the host OPP, and the LUMOs of the two complexes are completely derived from the LUMO of the guest endofullerene $Y_3N@C_{80}$. Namely, the LUMO level of the free $Y_3N@C_{80}$ can be raised by noncovalent binding with the nanoring, which may be very significant for endofullerene as a promising potential electron-accepting component in high-performance solar cells.[47] It is worth noting that for both $Y_3N@C_{80}$⊂OPP and $2Y_3N@C_{80}$⊂OPP, their gap values are almost the same as those of $Y_3N@C_{80}$, which indicates that the electronic properties of the complexes may heavily depend on the guest molecule.

To further reveal the electronic behavior and properties of supramolecular complexes, the ionization potential (IP) and the electron affinity (EA) were calculated, where the IP and EA were specified from the energies of the corresponding charged and neutral species. Table 2 presents the calculated values of

**Table 2. Vertical Ionization Potentials ($IP_v$, eV), Adiabatic Ionization Potentials ($IP_a$, eV), Vertical Electron Affinity ($EA_v$, eV), and Adiabatic Electron Affinity ($EA_a$, eV)**

| systems | $IP_v$ | $IP_a$ | $EA_v$ | $EA_a$ |
|---|---|---|---|---|
| OPP | 5.76 | 5.72 | 1.20 | 1.36 |
| $Y_3N@C_{80}$ | 6.65 | 6.63 | 1.97 | 2.02 |
| $Y_3N@C_{80}$⊂OPP | 5.83 | 5.77 | 1.82 | 1.89 |
| $2Y_3N@C_{80}$⊂OPP | 5.86 | 5.81 | 2.12 | 2.17 |

vertical ionization energy ($IP_v$), adiabatic ionization energy ($IP_a$), vertical electron affinity ($EA_v$), and adiabatic electron affinity ($EA_a$) for OPP, $Y_3N@C_{80}$, and their supramolecular complexes. The results indicate that the IP and EA of free $Y_3N@C_{80}$ are both higher than those of free OPP, indicating that OPP exhibited a stronger electron-donating capacity but a weaker electron-accepting capacity than $Y_3N@C_{80}$ in their isolated states. A comparison shows that the electrons in the supramolecular complexes $Y_3N@C_{80}$⊂OPP and $2Y_3N@C_{80}$⊂OPP are more bonded than free OPP and have a much stronger capacity to capture an additional electron since both the IP and EA of the complexes are larger than those of the free OPP. These findings suggest that encapsulating $Y_3N@C_{80}$ in OPP to form complexes is an effective way to change the electronic properties of OPP.

In supramolecular systems, charge transfer is a common phenomenon that can stabilize the resulting complexes. The magnitude of charge transfer is largely determined by the distance and orientation between the molecules, as well as the electron affinity of the acceptor molecule. The formation of charge transfer complexes can influence the electronic structure and properties of the individual molecules involved, leading to changes in their reactivity and optical properties.[48,49]

Table 3 presents the Mulliken and natural population atom (NPA) charge transfers between the host and guest molecules

**Table 3. Mulliken and Natural Population Analysis (NPA) Charge Transfers (e) between the Host and Guest at the B3LYP-D3/6-31G(d)∼SDD Level**

| complexes | NPA | Mulliken |
|---|---|---|
| $Y_3N@C_{80}$⊂OPP | 0.06 | 0.28 |
| $2Y_3N@C_{80}$⊂OPP | 0.11 | 0.56 |

during the formation of the two complexes. The results show that the Mulliken and NPA charge transfers for $Y_3N@C_{80}$⊂OPP are 0.28 and 0.06 e, respectively, leading to the formation of a polar complex, $Y_3N@C_{80}^{\delta-}$⊂$OPP^{\delta+}$. The charge transfer amount of the $Y_3N@C_{80}$⊂OPP as derived via Mulliken analysis is substantially larger than that of the [11]CPP−La@$C_{82}$ complex reported by Yamago et al.[10] More charge transfer is an indispensable factor for the stability of supramolecular complexes. Interestingly, the Mulliken and NPA charge transfers of the $2Y_3N@C_{80}$⊂OPP complex are 0.11 and 0.56 e, respectively, which are 2 times higher than those of $Y_3N@C_{80}$⊂OPP. This indicates that the amount of charge transfer between supramolecular complexes is intimately related to the number of guest molecules.

**3.4. Energy Decomposition Analysis and Weak Interaction Regions.** To determine the nature of weak interactions in supramolecular complexes, energy decomposition analysis based on the classical molecular force field (EDA-FF) was carried out with Multiwfn software. This method can decompose the weak interactions of the system into dispersion interactions, electrostatic interactions, and repulsive interac-


https://doi.org/10.1021/acsomega.3c02049
ACS Omega 2023, 8, 23754−23762

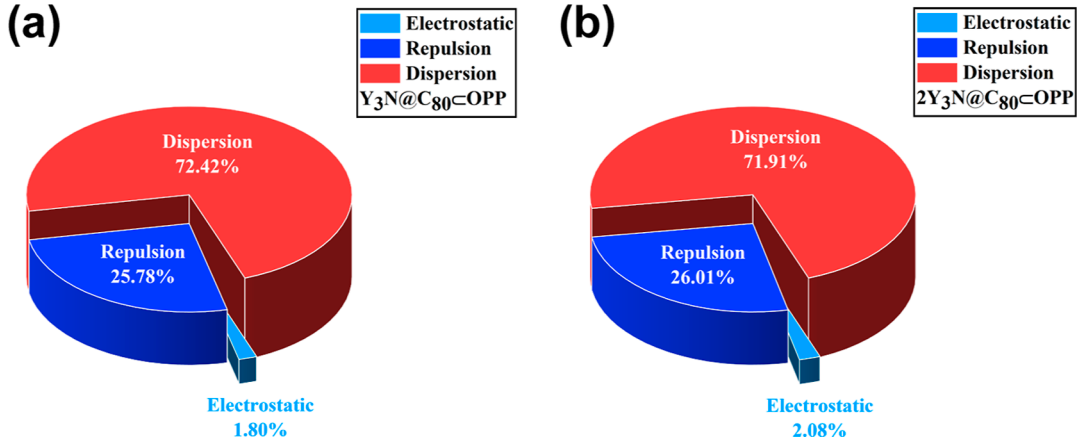


**Figure 5.** Schematic representation of the interaction energy decomposition of (a) $Y_3N@C_{80}⊂OPP$ and (b) $2Y_3N@C_{80}⊂OPP$ obtained from the EDA-FF analysis.

tions. The electrostatic interaction energy between atoms A and B ($E_{AB}^{ele}$) is shown below

$$E_{AB}^{ele} = \frac{q_A q_B}{r_{AB}} \quad (1)$$

where $q$ is the atomic charge, and $r_{AB}$ is the distance between A and B.

$E^{rep}$ is the repulsive interaction, and $E^{disp}$ is the attractive dispersion interaction. They are calculated as follows

$$E_{AB}^{rep} = \varepsilon_{AB}\left(\frac{R_{AB}^0}{r_{AB}}\right)^{12} \quad (2)$$

$$E_{AB}^{rep} = -2\varepsilon_{AB}\left(\frac{R_{AB}^0}{r_{AB}}\right)^{6} \quad (3)$$

where $\varepsilon_{AB}$ is the well depth of the interatomic van der Waals interaction potential, and $R_{AB}^0$ is the van der Waals nonbond distance. EDA-FF is highly dependent on interatomic and nonbond distances; therefore, we cannot be too demanding in terms of quantitative accuracy, but the relative contribution of each component is still helpful in understanding the nature of the intermolecular interactions.

The interaction energies for the $Y_3N@C_{80}⊂OPP$ and $2Y_3N@C_{80}⊂OPP$ systems obtained from EDA-FF were −211.78 and −414.87 kJ mol$^{-1}$, respectively. Although the results were different from those obtained from high-precision single-point energies performed at the ωB97M-V/def2-QZVPP level (see Table 1), the overall trend was the same for both. This suggests that the results of EDA-FF are plausible. The EDA-FF results are shown in Figure 5, and the detailed energies are shown in Table S2. As depicted in Figure 5, $Y_3N@C_{80}⊂OPP$ and $2Y_3N@C_{80}⊂OPP$ showed the same trend, namely, the electrostatic interaction accounted for the least (approximately 2%), while the dispersion interaction accounted for the most (more than 70%). This indicates that the dispersion interaction determines the stability of the complex, while the electrostatic interaction promotes its stability but is not a decisive factor. Generally, the larger the interaction energy ($E_{int}$) is, the more stable the system. The $E_{int}$ of $2Y_3N@C_{80}⊂OPP$ is approximately twice that of $Y_3N@C_{80}⊂OPP$, which indicates that the addition of $Y_3N@C_{80}$ enhances the stability of the system. Both systems are held together by π−π interactions, which also emphasizes the necessity of using dispersion corrections in the calculations.

IGMH is an intuitive method that visualizes the main interaction regions between specific fragments of a compound using the isosurface of the $\delta g^{inter}$ function. Figure 6 illustrates

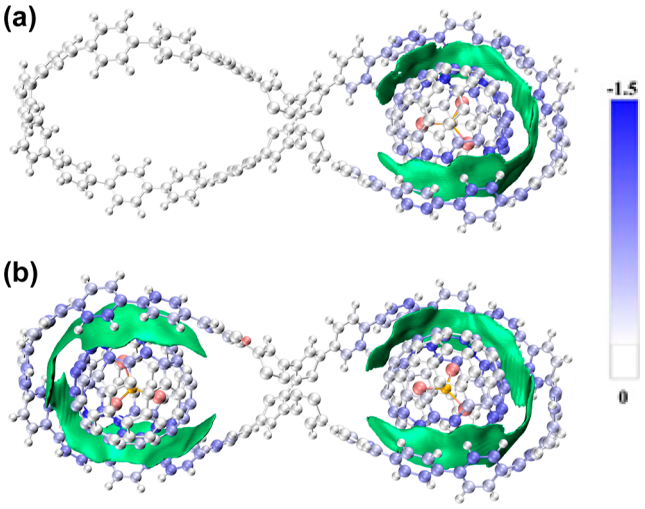


**Figure 6.** Visualized weak interaction regions with a $\delta g^{inter}$ isovalue of 0.001 a.u. of the (a) $Y_3N@C_{80}⊂OPP$ and (b) $2Y_3N@C_{80}⊂OPP$ systems. Atoms are colored by their contributions to the dispersion interaction between the host (OPP) and guest ($Y_3N@C_{80}$) according to the color bar. For clarity, the $Y_3N$ cluster is shown in pink and orange for Y and N atoms, respectively, rather than white. The color scale is given in kcal mol$^{-1}$.

the visualized weak interaction regions of the interaction between $Y_3N@C_{80}$ and OPP, where atoms in different segments are colored based on their contributions to the atom pair dispersion interaction energy (from EDA-FF). The method identifies the interaction between the host−guest molecules as a typical π−π stacking type, where the electronic density on the $\delta g^{inter}$ isosurface is small (approximately 0.001 a.u.), and the green isosurface can be recognized as a weak interaction region. As the interface distance between the host OPP and the guest $Y_3N@C_{80}$ decreases, the atoms become bluer, indicating stronger vdW π−π interactions. Conversely, the vdW π−π interaction no longer exists when the distance between atoms exceeds a certain threshold. It should be noted


https://doi.org/10.1021/acsomega.3c02049
ACS Omega 2023, 8, 23754−23762

that the weak interaction region between $Y_3N@C_{80}$⊂OPP is not closed, and the maximum distance of its unclosed area is much larger than the van der Waals contact distance between carbon atoms. As shown in Figure 2, the longest distance of the van der Waals interface is larger than 6 Å, and the vdW $\pi-\pi$ interaction will no longer exist. IGMH analysis confirms that this noncovalent interaction is mainly contributed by eight of the ten benzene rings surrounding the fullerene guest in each cavity, consistent with the system phenomenon of $2C_{60}$@OPP and $2C_{70}$@CPP studied by Zhan et al.[17] The IGMH not only visualizes the weak interaction regions but also identifies the weak interaction type as $\pi-\pi$ stacking interaction.

## 4. CONCLUSIONS

In this work, we computationally studied the structures and properties of the complexes formed by $Y_3N@C_{80}$ and OPP. Quantum chemical calculations demonstrate that the elastic adaptability and shape flexibility of OPP allow it to form a dimeric structure with $Y_3N@C_{80}$. The binding energy and thermodynamic data indicate that these complexes are highly stable and thermodynamically spontaneous. ESP analysis shows that the $Y_3N@C_{80}$ molecule would be oriented within OPP, thus allowing complementary ESP regions to be in close contact. Through a comprehensive investigation on the electronic properties of both the host and guest molecules, it is revealed that the addition of the $Y_3N@C_{80}$ guest would enhance the electron binding ability of the supramolecular system. The EDA-FF method indicates that the interaction between the host and guest molecules is dominated by dispersion attraction.

As research on concave−convex $\pi-\pi$ supramolecular systems develops in the future, metallofullerenes are undoubtedly one of the significant guest molecules that match well with nanorings, and the rich electronic and magnetic properties of metallofullerenes are expected to form more functional supramolecular complexes. The research results of this study help to better understand this type of host−guest system and promote the development of new supramolecular nanostructures.

## ■ ASSOCIATED CONTENT

### Supporting Information

The Supporting Information is available free of charge at https://pubs.acs.org/doi/10.1021/acsomega.3c02049.

Optimized geometries, geometric parameters, EDA-FF analysis, and coordinates for optimized compounds using the B3LYP-D3/6-31G*∼SDD level of theory (PDF)

## ■ AUTHOR INFORMATION


### Corresponding Authors

**Zhuxia Zhang** − *College of Chemistry, Taiyuan University of Technology, Taiyuan 030024, China;* orcid.org/0000-0003-3536-6363; Email: zhangzhuxia@tyut.edu.cn

**Taishan Wang** − *Beijing National Laboratory for Molecular Sciences, Key Laboratory of Molecular Nanostructure and Nanotechnology, Institute of Chemistry, Chinese Academy of Sciences, Beijing 100190, China;* orcid.org/0000-0003-1834-3610; Email: wangtais@iccas.ac.cn

### Authors

**Linshan Liu** − *Key Laboratory of Interface Science and Engineering in Advanced Materials, College of Materials Science and Engineering, Taiyuan University of Technology, Taiyuan 030024, China*

**Yang Liu** − *Key Laboratory of Interface Science and Engineering in Advanced Materials, College of Materials Science and Engineering, Taiyuan University of Technology, Taiyuan 030024, China*

Complete contact information is available at: https://pubs.acs.org/10.1021/acsomega.3c02049

### Author Contributions

‖L.L. and Y.L. contributed equally to this work.


### Notes

The authors declare no competing financial interest.

## ■ ACKNOWLEDGMENTS

This work was supported by the National Natural Science Foundation of China (51972309).

## ■ REFERENCES


(1) Popov, A. A.; Yang, S.; Dunsch, L. Endohedral fullerenes. *Chem. Rev.* **2013**, *113*, 5989−6113.

(2) Kroto, H. W.; Heath, J. R.; O'Brien, S. C.; Curl, R. F.; Smalley, R. E. C60: Buckminsterfullerene. *Nature* **1985**, *318*, 162−163.

(3) Billups, W. E. Fullerenes: Chemistry and reactions by andreas hirsch and michael brettreich (friedrich alexander university of erlangen-nuremberg). Wiley-vch verlag gmbh & co. Kgaa: Weinheim, germany. 2005. Xviii + 423 pp. $180.00. Isbn 3-527-30820-2. *J. Am. Chem. Soc.* **2005**, *127*, 11876.

(4) Zhou, C.; Zhen, M.; Yu, M.; Li, X.; Yu, T.; Liu, J.; Jia, W.; Liu, S.; Li, L.; Li, J.; Sun, Z.; Zhao, Z.; Wang, X.; Zhang, X.; Wang, C.; Bai, C. Gadofullerene inhibits the degradation of apolipoprotein b100 and boosts triglyceride transport for reversing hepatic steatosis. *Sci. Adv.* **2020**, *6*, No. eabc1586.

(5) Perez, E. M.; Martin, N. $\pi-\pi$ interactions in carbon nanostructures. *Chem. Soc. Rev.* **2015**, *44*, 6425−6433.

(6) Kawase, T.; Kurata, H. Ball-bowl-and belt-shaped conjugated systems and their complexing abilities: Exploration of the concave-convex pi-pi interaction. *Chem. Rev.* **2006**, *106*, 5250−5273.

(7) Iwamoto, T.; Watanabe, Y.; Sadahiro, T.; Haino, T.; Yamago, S. Size-selective encapsulation of c60 by [10]cycloparaphenylene: Formation of the shortest fullerene-peapod. *Angew. Chem., Int. Ed.* **2011**, *50*, 8342−8344.

(8) Stergiou, A.; Rio, J.; Griwatz, J. H.; Arcon, D.; Wegner, H. A.; Ewels, C. P.; Tagmatarchis, N. A long-lived azafullerenyl radical stabilized by supramolecular shielding with a [10]cycloparaphenylene. *Angew. Chem., Int. Ed.* **2019**, *58*, 17745−17750.

(9) Iwamoto, T.; Watanabe, Y.; Takaya, H.; Haino, T.; Yasuda, N.; Yamago, S. Size- and orientation-selective encapsulation of c(70) by cycloparaphenylenes. *Chemistry* **2013**, *19*, 14061−14068.

(10) Iwamoto, T.; Slanina, Z.; Mizorogi, N.; Guo, J.; Akasaka, T.; Nagase, S.; Takaya, H.; Yasuda, N.; Kato, T.; Yamago, S. Partial charge transfer in the shortest possible metallofullerene peapod, la@c82 subset[11]cycloparaphenylene. *Chemistry* **2014**, *20*, 14403−14409.

(11) Nakanishi, Y.; Omachi, H.; Matsuura, S.; Miyata, Y.; Kitaura, R.; Segawa, Y.; Itami, K.; Shinohara, H. Size-selective complexation and extraction of endohedral metallofullerenes with cycloparaphenylene. *Angew. Chem., Int. Ed.* **2014**, *53*, 3102−3106.

(12) Chen, H.; Gui, S.; Zhang, Y.; Liu, Z.; Miao, Q. Synthesis of a hydrogenated zigzag carbon nanobelt. *CCS Chem.* **2021**, *3*, 613−619.

(13) Huang, Z. A.; Chen, C.; Yang, X. D.; Fan, X. B.; Zhou, W.; Tung, C. H.; Wu, L. Z.; Cong, H. Synthesis of oligoparaphenylene-

derived nanohoops employing an anthracene photodimerization-cycloreversion strategy. *J. Am. Chem. Soc.* **2016**, *138*, 11144−11147.
(14) Sun, Z.; Ikemoto, K.; Fukunaga, T. M.; Koretsune, T.; Arita, R.; Sato, S.; Isobe, H. Finite phenine nanotubes with periodic vacancy defects. *Science* **2019**, *363*, 151−155.
(15) Li, P.; Zakharov, L. N.; Jasti, R. A molecular propeller with three nanohoop blades: Synthesis, characterization, and solid-state packing. *Angew. Chem., Int. Ed.* **2017**, *56*, 5237−5241.
(16) Zhang, W.; Abdulkarim, A.; Golling, F. E.; Rader, H. J.; Mullen, K. Cycloparaphenylenes and their catenanes: Complex macrocycles unveiled by ion mobility mass spectrometry. *Angew. Chem., Int. Ed.* **2017**, *56*, 2645−2648.
(17) Zhan, L.; Dai, C.; Zhang, G.; Zhu, J.; Zhang, S.; Wang, H.; Zeng, Y.; Tung, C. H.; Wu, L. Z.; Cong, H. A conjugated figure-of-eight oligoparaphenylene nanohoop with adaptive cavities derived from cyclooctatetrathiophene core. *Angew. Chem., Int. Ed.* **2022**, *61*, No. e202113334.
(18) Liang, J.; Lu, Y.; Zhang, J.; Qiu, L.; Li, W.; Zhang, Z.; Wang, C.; Wang, T. Visible and near-infrared photoluminescence of a supramolecular complex constructed from a cycloparaphenylene nanoring and an erbium metallofullerene. *Dalton Trans.* **2022**, *51*, 10227−10233.
(19) Liu, Y.; Li, W.; Li, P.; Guo, Y.; Cui, P.; Zhang, Z. Theoretical exploration of noncovalent interactions in $Sc_2C_2@C_{2n}$ (n = 40, 41, and 42)⊂[12]CPP, PF[12]CPP. *RSC Adv.* **2023**, *13*, 4553−4563.
(20) Lu, Y. X.; Zhao, C.; Zhang, J.; Li, W.; Liang, J. Y.; Liu, L. S.; Li, Y. G.; Wang, C. R.; Wang, T. S. A molecular brake hoop for the motion of metal atoms inside fullerene cage. *Sci. China: Chem.* **2022**, *65*, 1601−1606.
(21) Lu, Y. X.; Zhao, C.; Zhang, J.; Li, W.; Liu, L. S.; Zheng, C. F.; Wang, C. R.; Wang, T. S. Enhanced spin-nuclei couplings of paramagnetic azametallofullerene hooped in cycloparaphenylene. *J. Phys. Chem. C* **2023**, *127*, 4660−4664.
(22) Nie, M.; Liang, J.; Zhao, C.; Lu, Y.; Zhang, J.; Li, W.; Wang, C.; Wang, T. Single-molecule magnet with thermally activated delayed fluorescence based on a metallofullerene integrated by dysprosium and yttrium ions. *ACS Nano* **2021**, *15*, 19080−19088.
(23) Zhang, J.; Qiu, Z. L.; Zhao, C.; Lu, Y. X.; Li, W.; Liu, L. S.; Wang, C. R.; Tan, Y. Z.; Wang, T. S. Synergistic modulation of spin and fluorescence signals in a nano-saturn assembled by a metallofullerene and cycloparaphenylene nanohoop. *Nano Res.* **2022**, *16*, 3372−3378.
(24) Zhao, C.; Meng, H.; Nie, M.; Huang, Q.; Du, P.; Wang, C.; Wang, T. Construction of a short metallofullerene-peapod with a spin probe. *Chem. Commun.* **2019**, *55*, 11511−11514.
(25) Zhao, C.; Meng, H.; Nie, M.; Wang, X.; Cai, Z.; Chen, T.; Wang, D.; Wang, C.; Wang, T. Supramolecular complexes of c80-based metallofullerenes with [12]cycloparaphenylene nanoring and altered property in a confined space. *J. Phys. Chem. C* **2019**, *123*, 12514−12520.
(26) Dias, F. B.; Penfold, T. J.; Monkman, A. P. Photophysics of thermally activated delayed fluorescence molecules. *Methods Appl. Fluoresc.* **2017**, *5*, 012001.
(27) Liang, J.; Wang, C.; Wang, T. Studies on the luminescence property of yttrium-based metallofullerenes. *Chin. J. Struct. Chem.* **2022**, *41*, 2209001−2209007.
(28) Becke, A. D. Density-functional exchange-energy approximation with correct asymptotic behavior. *Phys. Rev. A: At., Mol., Opt. Phys.* **1988**, *38*, 3098−3100.
(29) Hariharan, P. C.; Pople, J. A. The influence of polarization functions on molecular orbital hydrogenation energies. *Thermochim. Acta* **1973**, *28*, 213−222.
(30) Andrae, D.; Huermann, U.; Dolg, M.; Stoll, H.; Preu, H. Energy-adjustedab initio pseudopotentials for the second and third row transition elements. *Thermochim. Acta* **1990**, *77*, 123−141.
(31) Grimme, S.; Antony, J.; Ehrlich, S.; Krieg, H. A consistent and accurate ab initio parametrization of density functional dispersion correction (dft-d) for the 94 elements h-pu. *J. Chem. Phys.* **2010**, *132*, 154104.
(32) Frisch, M. J.; Trucks, G. W.; Schlegel, H. B.; Scuseria, G. E.; Robb, M. A.; Cheeseman, J. R.; Scalmani, G.; Barone, V.; Petersson, G. A.; Nakatsuji, H.; Li, X.; Caricato, M.; Marenich, A. V.; Bloino, J.; Janesko, B. G.; Gomperts, R.; Mennucci, B.; Hratchian, H. P.; Ortiz, J. V.; Izmaylov, A. F.; Sonnenberg, J. L.; Williams; Ding, F.; Lipparini, F.; Egidi, F.; Goings, J.; Peng, B.; Petrone, A.; Henderson, T.; Ranasinghe, D.; Zakrzewski, V. G.; Gao, J.; Rega, N.; Zheng, G.; Liang, W.; Hada, M.; Ehara, M.; Toyota, K.; Fukuda, R.; Hasegawa, J.; Ishida, M.; Nakajima, T.; Honda, Y.; Kitao, O.; Nakai, H.; Vreven, T.; Throssell, K.; Montgomery, J. A., Jr.; Peralta, J. E.; Ogliaro, F.; Bearpark, M. J.; Heyd, J. J.; Brothers, E. N.; Kudin, K. N.; Staroverov, V. N.; Keith, T. A.; Kobayashi, R.; Normand, J.; Raghavachari, K.; Rendell, A. P.; Burant, J. C.; Iyengar, S. S.; Tomasi, J.; Cossi, M.; Millam, J. M.; Klene, M.; Adamo, C.; Cammi, R.; Ochterski, J. W.; Martin, R. L.; Morokuma, K.; Farkas, O.; Foresman, J. B.; Fox, D. J. *Gaussian 09*, Rev. D.01; Gaussian Inc.: Wallingford CT, 2013.
(33) Mardirossian, N.; Head-Gordon, M. ωb97m-v: A combinatorially optimized, range-separated hybrid, meta-gga density functional with vv10 nonlocal correlation. *J. Chem. Phys.* **2016**, *144*, 214110.
(34) Weigend, F.; Ahlrichs, R. Balanced basis sets of split valence, triple zeta valence and quadruple zeta valence quality for H to Rn: Design and assessment of accuracy. *Phys. Chem. Chem. Phys.* **2005**, *7*, 3297−3305.
(35) Mardirossian, N.; Head-Gordon, M. Thirty years of density functional theory in computational chemistry: an overview and extensive assessment of 200 density functionals. *Mol. Phys.* **2017**, *115*, 2315−2372.
(36) Neese, F. Software update: The ORCA program system—Version 5.0. *Wiley Interdiscip. Rev.: Comput. Mol. Sci.* **2022**, *12*, No. e1606.
(37) Kossmann, S.; Neese, F. Comparison of two efficient approximate hartee−fock approaches. *Chem. Phys. Lett.* **2009**, *481*, 240−243.
(38) Zhang, J.; Lu, T. Efficient evaluation of electrostatic potential with computerized optimized code. *Phys. Chem. Chem. Phys.* **2021**, *23*, 20323−20328.
(39) Lu, T.; Liu, Z.; Chen, Q. Comment on "18 and 12—member carbon rings (cyclo[n]carbons)—a density functional study". *Mater. Sci. Eng., B* **2021**, *273*, 115425.
(40) Lu, T.; Chen, Q. Independent gradient model based on hirshfeld partition: A new method for visual study of interactions in chemical systems. *J. Comput. Chem.* **2022**, *43*, 539−555.
(41) Lu, T.; Chen, F. Multiwfn: A multifunctional wavefunction analyzer. *J. Comput. Chem.* **2012**, *33*, 580−592.
(42) Lu, T.; Chen, Q. Shermo: A general code for calculating molecular thermochemistry properties. *Comput. Theor. Chem.* **2021**, *1200*, 113249.
(43) Gonzalez-Veloso, I.; Cabaleiro-Lago, E. M.; Rodriguez-Otero, J. Fullerene size controls the selective complexation of [11]cpp with pristine and endohedral fullerenes. *Phys. Chem. Chem. Phys.* **2018**, *20*, 11347−11358.
(44) Gonzalez-Veloso, I.; Rodriguez-Otero, J.; Cabaleiro-Lago, E. M. Carbon-nanorings ([10]cpp and [6]cppa) as fullerene (c(60) and c(70)) receptors: A comprehensive dispersion-corrected dft study. *Phys. Chem. Chem. Phys.* **2016**, *18*, 31670−31679.
(45) Cabaleiro-Lago, E. M.; Rodríguez-Otero, J.; Carrazana-García, J. A. A theoretical study of complexes between fullerenes and concave receptors with interest in photovoltaics. *Phys. Chem. Chem. Phys.* **2017**, *19*, 26787−26798.
(46) George, G.; Stasyuk, O. A.; Voityuk, A. A.; Stasyuk, A. J.; Sola, M. Aromaticity controls the excited-state properties of host-guest complexes of nanohoops. *Nanoscale* **2023**, *15*, 1221−1229.
(47) He, Y.; Chen, H. Y.; Hou, J.; Li, Y. Indene-c(60) bisadduct: A new acceptor for high-performance polymer solar cells. *J. Am. Chem. Soc.* **2010**, *132*, 1377−1382.
(48) Goetz, K. P.; Tsutsumi, J.; Pookpanratana, S.; Chen, J. H.; Corbin, N. S.; Behera, R. K.; Coropceanu, V.; Richter, C. A.; Hacker, C. A.; Hasegawa, T.; Jurchescu, O. D. Reply to comment on polymorphism in the 1:1 charge-transfer complex dbttf-tcnq and its


https://doi.org/10.1021/acsomega.3c02049
*ACS Omega* 2023, 8, 23754−23762

effects on optical and electronic properties. *Adv. Electron. Mater.* **2017**, *3*, 1600521.
(49) Abimannan, G.; Sengodan, P.; Ravichandran, S.; Mary Anjalin, F.; Kumar, K. A. R.; Maadeswaran, P. Structural, optical, morphological and charge transfer properties of ceo2/mwcnts nanocomposite and their photocatalytic activity of organic dye degradation. *J. Sol-Gel Sci. Technol.* **2023**, *105*, 625−636.



https://doi.org/10.1021/acsomega.3c02049
*ACS Omega* 2023, 8, 23754−23762